Chapter 4:

Studies of Guest Cobalt Schiff-base Complexes Entrapped in Zeolite Y and their Catalytic Activity for the Degradation of Rhodamine B dye

Chapter 4

***Abstract**: Planar Co(II)–Schiff base complexes show the modified structural and functional properties after encapsulation inside zeolite-Y. In the free-state, the reactivity of the Co(II)-Schiff base complexes is mainly controlled by the electronic effect of the different substituent groups present in the complex. But after the encapsulation in zeolite Y, reactivity is modified and determined by the altered electron density around metal center. All the systems are well characterized with the help of different characterization tools like XRD analysis, SEM-EDX, FTIR, XPS, TGA, BET and UV Visible spectroscopy and the comparative studies of structural and catalytic modifications have delivered a rational explanation of enhanced reactivity of zeolite encapsulated metal complexes for the degradation of rhodamine B dye as compared to their corresponding free-states.*

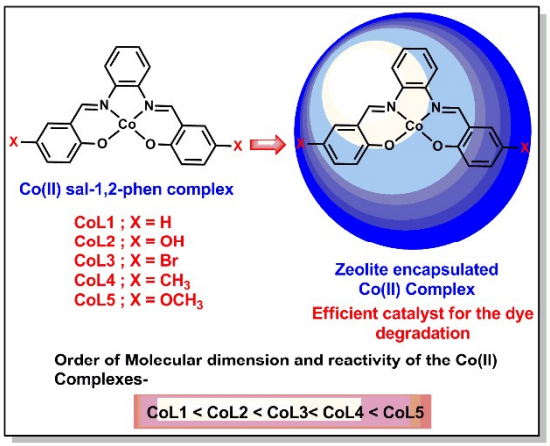

*S. Kumari and S. Ray, Cobalt Schiff-base Complexes Encapsulated in Zeolite Y and their Catalytic Activity for the Degradation of Rhodamine B, *(to be communicated)*.

4.1 INTRODUCTION

Now a days, textile industries release waste water which acts as pollutants as it contains organic dyes. Esthetic pollution, eutrophication and perturbations are the most common adverse effects due to release of dyes contaminated waste water in the ecosystem. Dyes are mostly non -biodegradable and various N-containing dyes for example rhodamine B (RhB) undergoes natural reductive anaerobic degradation to produce eventually carcinogenic aromatic amines.[1]

Transition metal complexes play a significant role in the era of catalysis and photocatalysis for the oxidation, reduction and polymerization reactions etc.[2-4] However, these complexes are very difficult to separate and recover from the reaction medium. Therefore, researchers become attentive to heterogenization of these homogenous catalysts to overcome these challenges.[5, 6]

However, cobalt(II) based systems is an alternative of highly expensive metals such as titanium which is commonly used for the degradation of dyes, because cobalt(II) based systems impart enhanced catalytic activity Towards heterogenization, immobilization and encapsulation of homogeneous transition metal complexes into zeolites, MCM 41, polymer or a solid support have been executed.[7] Due to low cost and specific and precise architectural phenomenon, zeolite Y becomes a fascinating aluminosilicate material for encapsulating transition metal complexes. Over the past few decades, it has been observed that the immobilized 'ship in a bottle' metal complexes in inorganic porous materials conserve most of their solution phase properties and acquire stability along with size and shape selectivity. These encapsulated metal complexes therefore, can be used effectively for photo oxidation reactions. These hybrid systems exhibit more advantages over their homogeneous analogues and can be employed as effective eco-friendly catalyst to oxidize high toxic pollutants. Photocatalytic degradation of dye accompanies with electron-hole pair generation and subsequently the electron is captured by the catalyst. The zeolite encapsulated metal complex catalysts undergo alteration of band gap between HOMO and LUMO energy levels which eventually promotes the electron capture Therefore, these systems prevent the electron–hole recombination in the dye and hence facilitate the degradation process.[8] Furthermore, the zeolite encapsulated systems support the photo induced electron-transfer reactions to generate photoactive, powerful oxidative ion radical species for example $^{\bullet}OH$, $^{-}O_2$, and $^{+\bullet}O_2H$. These systems can enhance the photocatalytic degradation of various dyes (RhB, methyl orange, cango red) in presence of as green oxidant i.e., 30% H_2O_2 by the production of powerful active radical (E^o = $^{\bullet}OH$)

(E^o = 2.8 V)[9] and enhance the rate of the reaction. They are even efficient to degrade the carcinogenic xanthene class of dyes.[10]

Metal complexes containing N_2O_2 coordination sites, has grabbed considerable attention due to their various application such as catalysts, [11, 12] functional materials, non-linear optical materials,[13] molecular magnetism,[14] and organic electronics,[15] light emitting diodes[16] and display magnetic properties.[17] Co(II)-Schiff-base complexes containing N_2O_2 coordination sites, also find their applications in different catalytic reactions.[18] However, there are limited literature reports focusing on their applications on the dye degradation processes.[19] Arani *et al*. has reported the use of cobalt vanadate nanostructures in the photocatalytic degradation of organic dyes.[20] Fiber supported cobalt phthalocyanine system has been found efficiently active for the catalytic oxidation of organic dyes into small biodegradable compounds.[21]

Researchers have pursued investigation on the encapsulated metal complexes and found as efficient catalysts for variety of oxidation reactions.[22-24] Zeolite framework can substitute the protein mantle of natural enzymes and influence the reactivity similarly by way enzymes do.[25-27] Encapsulation can prevent multi-molecular deactivation pathways due to site isolation.[28] It is quite evident that these hybrid systems showcase the properties of their host, like nanocavity size, electrostatic potential, along with the electronic and stereo chemical properties of the guest complex.[29, 30]

Coming to the cobalt macrocyclic complexes, they usually display dimerization, and this affects the lifetime and stability of the cobalt catalytic systems. To enhance the activity of the cobalt complexes, preventing dimerization and degradation are mandatory. Therefore, catalytic activity Co(II) Schiff-base complexes can be escalated significantly by entrapping them in zeolitic cavity by preventing dimerization.

In the current study, a series of Co(II) salophen complexes are synthesized and also encapsulated within the supercage of zeolite-Y via flexible ligand method. With the aim of generating improved photocatalysts and to gain the insight of the catalytic processes, these systems are employed as catalysts for the photocatalytic degradation of rhodamine B dye (shown in Figure 4.1). With the help of different spectroscopy and detailed comparative catalytic studies of both the free and encapsulated cobalt complexes, the comprehension of correlation between structural modification and photocatalytic activity of these compounds have been targeted.

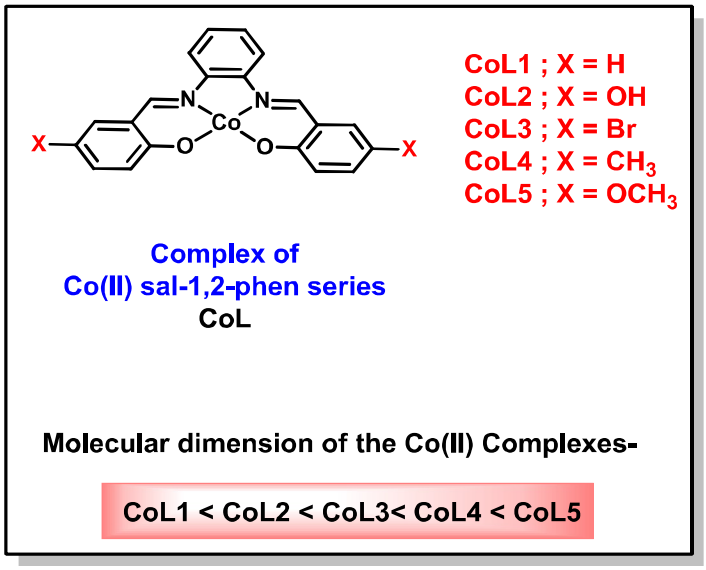

Figure 4.1: Schematic representation of cobalt Schiff-base complexes.

4.2 RESULTS AND DISCUSSION

Synthesis of ligands and copper Schiff-base complexes in free or encapsulated states have already been discussed in chapter 2 under experimental section (2.2.1-2.2.5).

4.2.1 Elemental Analysis

The elements present in the encapsulated cobalt complexes and Co(II)- exchanged zeolite Y have been confirmed by the Energy Dispersive X-ray (EDX) spectroscopy. The results obtained from elemental analysis are presented in Table 4.1. The Si/Al of pure zeolite-Y is found to be 2.7, representing the unit cell formula of parent zeolite Y as $Na_{52}(AlO_2)_{52}(SiO_2)_{140}.yH_2O$. However, the Si/Al ratio has been slightly altered during cobalt exchange and encapsulation process, indicating marginal dealumination during the encapsulation process. The cobalt metal content in all the encapsulated cobalt complexes has been found comparatively lesser without any exception with respect to that in Co(II) exchanged zeolite -Y. The decline in the cobalt content during the synthesis of complex within the supercage of zeolite Y is an indirect indication of the complex formation in the cavities of zeolite-Y. These results indicate that Soxhlet extraction has effectively removed the complexes adsorbed on the surface of host framework, and

subsequently, resulted the reduction of concentration of cobalt metal as compared to the Co-exchanged zeolite Y.

Table 4.1: Concentration of cobalt (wt %) content in the different Samples.

S.No.	Samples	Cobalt (wt%)	Si/ Al ratio
1	Zeolite-Y	-	2.79
2	Co-Y	2.12	2.79
3	CoL1-Y	0.51	2.78
4	CoL2-Y	0.52	2.78
5	CoL3-Y	0.54	2.79
6	CoL4-Y	0.54	2.78
7	CoL5-Y	0.54	2.78

4.2.2 X-Ray Diffraction (XRD) studies

The powder X-ray diffraction (PXRD) analysis has been carried out for pure zeolite-Y, Co(II)- exchanged zeolite-Y and zeolite encapsulated cobalt systems to prove the crystallinity and integrity of zeolite host framework (PXRD patterns shown in Figure 4.2). The similar XRD patterns of all encapsulated systems prove the retention of crystalline structure of host framework during the whole encapsulation process. However, variant diffraction intensities at (220) and (311) planes appearing at 2θ of 10° and 12° respectively has been noticed. In case of pure zeolite-Y and Co(II) exchanged zeolite, the intensity of I_{220} is greater than I_{311} and vice versa for all encapsulated cobalt systems. Such type of results already has been notified and empirically correlated with the existence of large molecule within the supercage of zeolite-Y.[31, 32] Such type of observations never perceived when formation of the complex occurs on the surface of the host framework.[33, 34] These results once again, prove the successful encapsulation of Co(II) complexes inside the supercage of zeolite-Y.

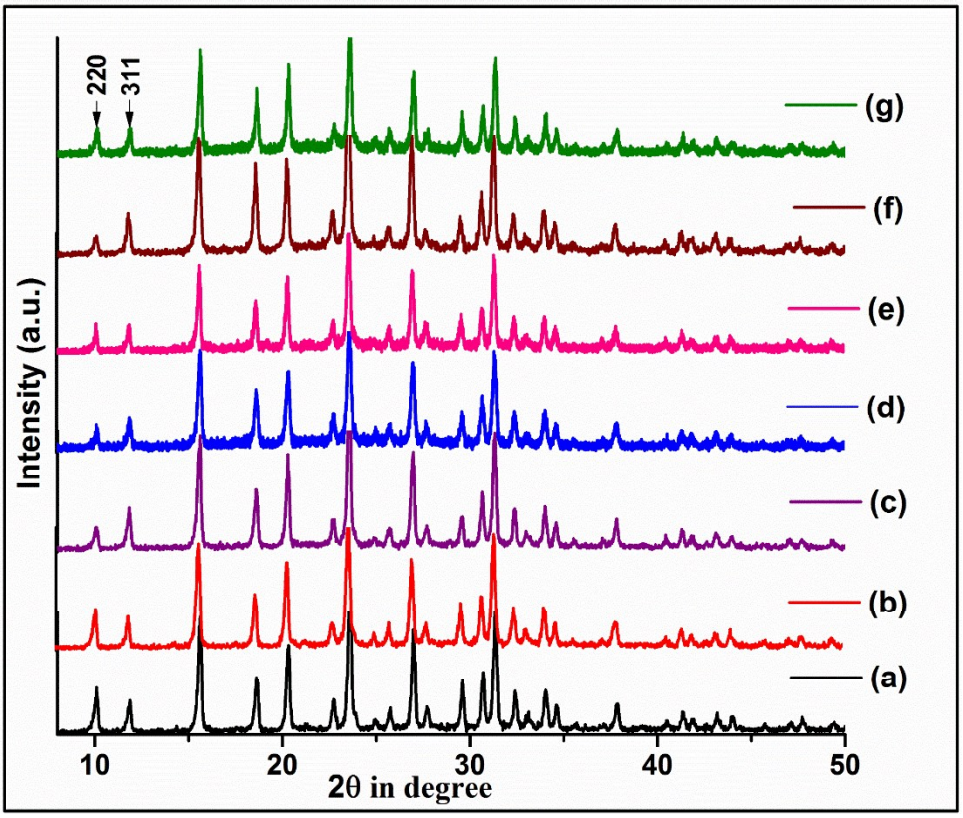

Figure 4.2: Powder XRD patterns of (a) pure zeolite-Y (b) Co- exchanged zeolite-Y, (c) CoL1-Y, (d) CoL2-Y, (e) CoL3-Y, (f) CoL4-Y and (g) CoL5-Y.

4.2.3 Scanning Electron Microscopy (SEM)

Synthesis of Co(II) salophen complexes within the supercage of zeolite framework has been performed with the help of 'flexible ligand method'. It is practically very difficult to synthesize the metal complex only within the supercage because some of these metal complexes certainly get synthesized and remain adsorbed on the surface of zeolite framework. Therefore, Soxhlet extraction becomes mandatory to remove impurities as on the surface, substantial amount of ligand species remain uncoordinated. To know the surface morphology of the zeolite framework, scanning electron (SE) micrographs of zeolite encapsulated systems have been taken before and after Soxhlet extraction (SEM images of zeolite encapsulated cobalt complex shown in Figure 4.3). In the images, presence of surface impurities become evident as for zeolites with encapsulated complex before Soxhlet extraction, impurities are clearly visible

on the surface of host framework. After Soxhlet extraction, the clear boundaries of the host particles and final pale yellow color of the encapsulated systems are apparent for the successful synthesis of metal complex only within the supercages of host.

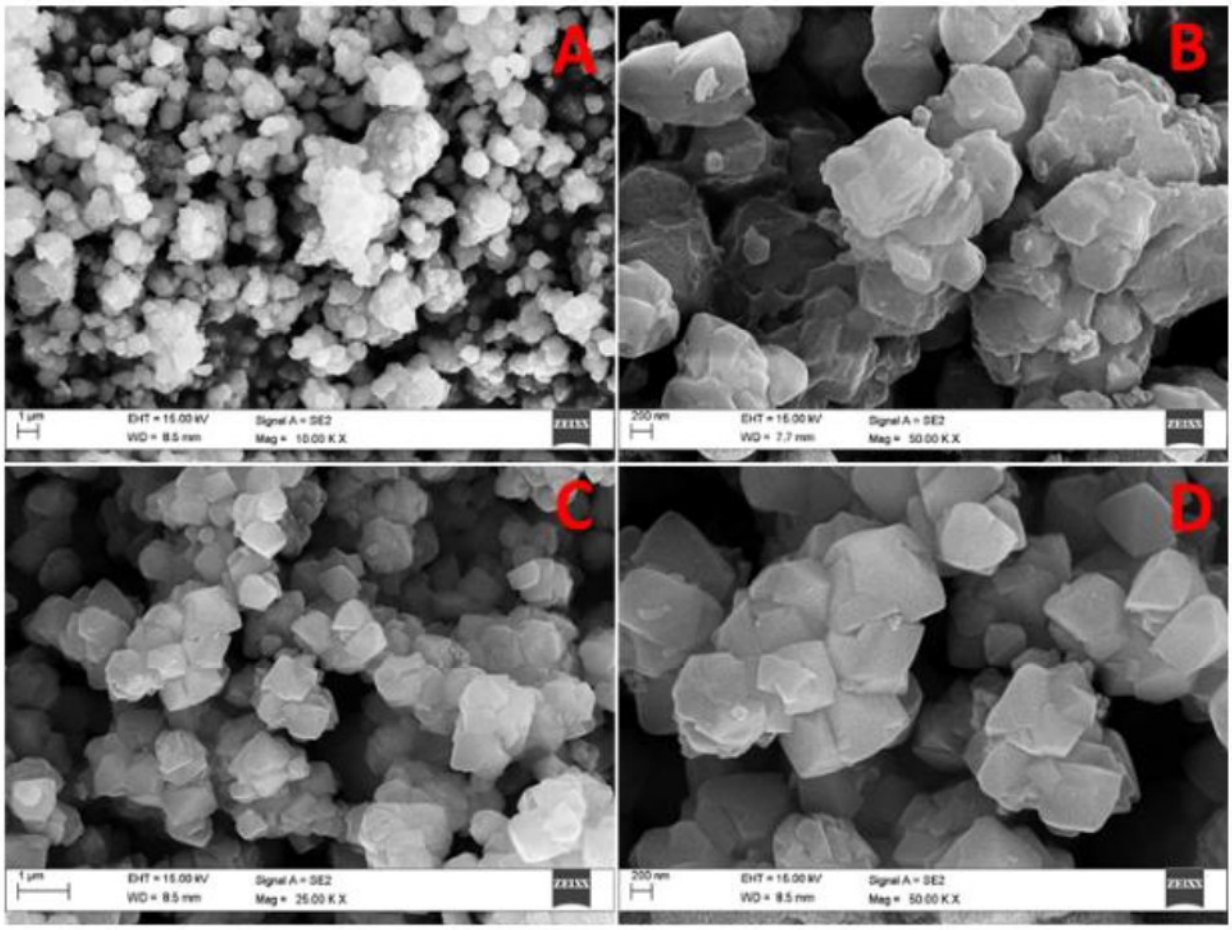

Figure 4.3: SEM images before Soxhlet extraction (A-B) CoL5-Y with different resolution, and after Soxhlet extraction (C-D) CoL5-Y.

4.2.4 BET surface area analysis

BET surface area analysis is quite relevant as a support of successful encapsulation of Co(II) Schiff-base complex within the supercage of zeolite-Y. The N_2 adsorption-desorption isotherms of pure zeolite-Y and

zeolite encapsulated Co(II) Schiff-base complexes are shown in Figure 4.4 and Table 4.2. N_2 adsorption-desorption isotherms for pure zeolite-Y and encapsulated cobalt complexes indicate type I isotherms which proves the microporous nature of materials.[35, 36] A distinctive though expected observation emerges from the comparative studies of pore volume and surface area of pure zeolite-Y and with encapsulated cobalt complex. The presence of cobalt Schiff -base complexes within the supercage of zeolite-Y is well supported by the decline of the pore volume and surface area of parent zeolite-Y upon encapsulation process.[37] The loading level of metal along with the size of complex within the host framework actually are the decisive factors for the decrease in BET surface area and pore volume upon encapsulation.

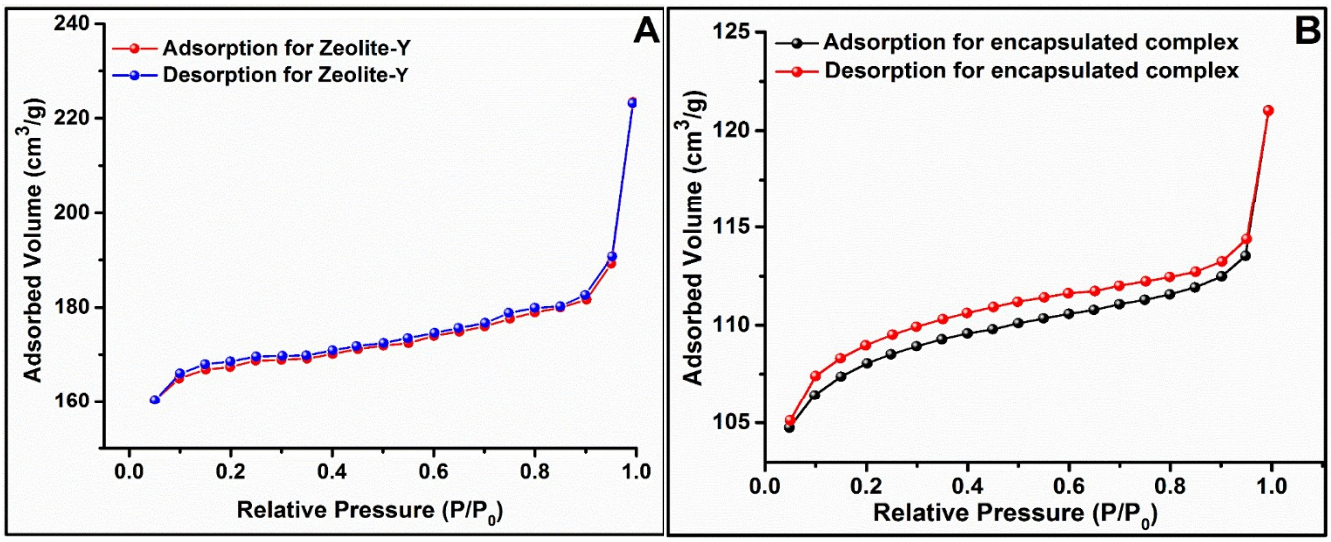

Figure 4.4: BET isotherms for pure zeolite-Y and zeolite encapsulated complex CoL5-Y.

Table 4.2: BET surface area and pore volume of pure zeolite Y and encapsulated cobalt complex (CoL5-Y).

S.No.	Sample	BET surface area (m^2/g)	Pore volume (cm^3/g)
1	**Pure zeolite Y**	535	0.3456
2	**CoL5-Y**	325	0.1825

4.2.5 Thermal analysis

To know the thermal stability of free-state and encapsulated cobalt complexes thermo-gravimetric analysis (TGA) has been performed. TGA experiment is carried out in the temperature range of (25-800) °C under nitrogen atmosphere along with 10°C/minute heating rate. The TGA results for free-state and encapsulated cobalt system are shown in Figure 4.5. The TGA analysis of zeolite entrapped cobalt complex stipulate two steps. First step occurs in the temperature range of (30 – 180) °C and is attributed to the loss of intrazeolite water molecules.[38] Second step arises in a broad temperature range of (300–750) °C indicating slow decomposition of chelating ligand. A very small weight loss actually suggests quite a low loading level of entrapped cobalt complex within the supercage of zeolite framework and these results are well-consistent with the weight% of cobalt metal estimated by the EDX analysis. Encapsulated cobalt complexes show that the weight loss temperature extends towards higher temperature, which indicates that the zeolite encaged cobalt complex is more thermally stabile as compared to the neat complexes.

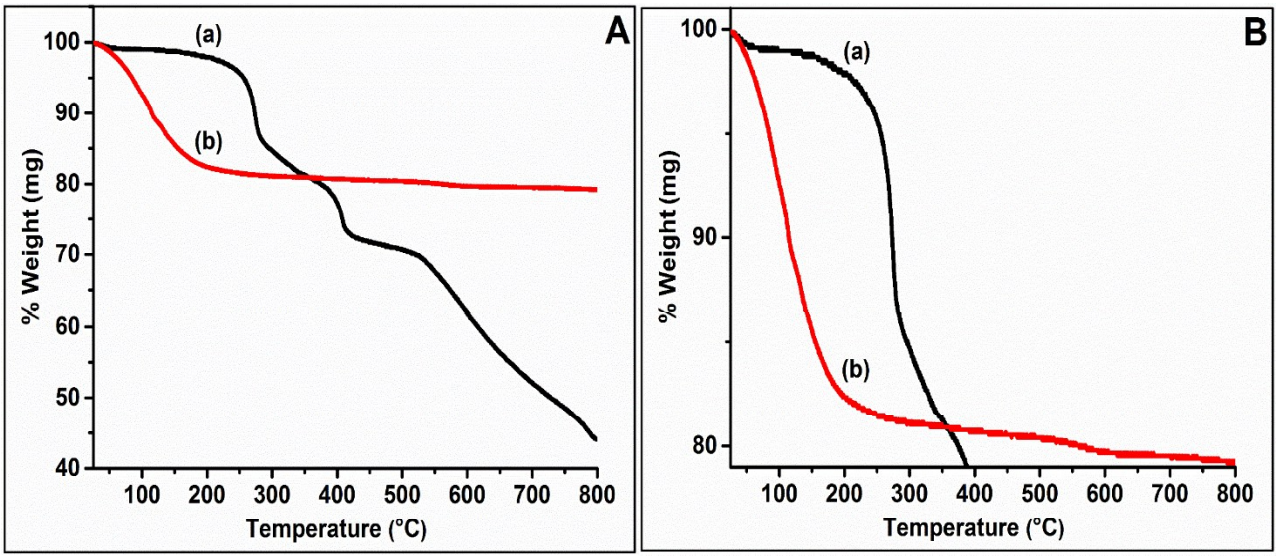

Figure 4.5: (A) TGA curves of (a) free-state CoL4 and (b) zeolite encapsulated CoL4-Y and (B) Enlarged view of TGA curves of (a) free-state CoL4 and (b) CoL4-Y.

4.2.6 Fourier Transform Infrared spectroscopy (FTIR)

The FTIR spectral data of pure zeolite-Y and encapsulated Co(II) Schiff-base complexes are presented in Figure 4.6. It is clear from the FTIR spectra that the characteristics IR bands of zeolite-Y dominate the spectra below 1200 cm^{-1}. FTIR spectra of pure zeolite Y (Figure 4.6) show strong IR peaks in the range 500−1200 cm^{-1}. The strong IR peak at the region 1010−1040 cm^{-1} attributed due to the asymmetric stretching vibrations of (Si/Al) O_4 units of zeolite framework. The prominent broad bands appeared at 1643 and 3500 cm^{-1} are assigned due to lattice water molecules and surface hydroxylic groups, respectively. Some other characteristics bands at 560, 717, and 786 cm^{-1} (Figure 4.6) are attributed to T−O bending mode, double ring and symmetric stretching vibrations respectively. These IR bands are not modified during the encapsulation process (Figure 4.6). The characteristic FTIR bands of zeolite framework remain unaltered during metal exchange reaction and encapsulation process implies that the zeolite framework maintains its integrity upon encapsulation of cobalt Schiff base complexes. However, there is noticeably a difference in the spectral range of 1200−1600 cm^{-1} for the encapsulated complex (see Figure 4.6). This region is suitable region for the study of encapsulated complexes because the zeolite framework does not show any absorption band and FTIR bands observed are only because of the complexes that lie in the range of 1200−1600 cm^{-1}. The IR peaks of encapsulated cobalt Schiff-base complex are very weak due to their low loading level in the zeolite supercage. The important FTIR bands are assigned in Table 4.3 for the both neat and encapsulated cobalt complexes.

Two strong FTIR bands of the ligands observed at 1612-1620 cm^{-1} and 1273-1296 $cm^{-1}$are correspond to the C=N and C-O stretching vibrations and these bands are slightly shifted towards lower frequency upon complexation, indicating nitrogen and oxygen coordination inside the cavity of zeolite Y. IR spectra of neat cobalt complex exhibit two strong bands at 1593-1609 cm^{-1} and 1257-1296 $cm^{-1}$are characteristic of C=N and C-O stretching vibrations. The bands at 1444- 1539 cm^{-1} are assigned to C=C stretching and peak at 1373-1396 cm^{-1} is attributed to ν_{C-H} deformation. In the FTIR spectra of encapsulated system, all IR bands are very less intense. This characteristic further reveals the nonexistence of extraneous metal complex on the external surface of zeolite-Y. The presence of similar FTIR vibrational bands in the neat and encapsulated complexes gives indirect evidence for the presence of a cobalt (II) Schiff base complex inside the super cage of zeolite. The slight shifting in the IR peak positions can be attributed due to the effect of zeolite framework on the geometry of the cobalt complexes trapped in the zeolite cavities. The

shift in ν_{C-H} deformation frequency after encapsulation of metal complex provides the evidence for the encapsulation of metal complex inside the cavity of zeolite Y.

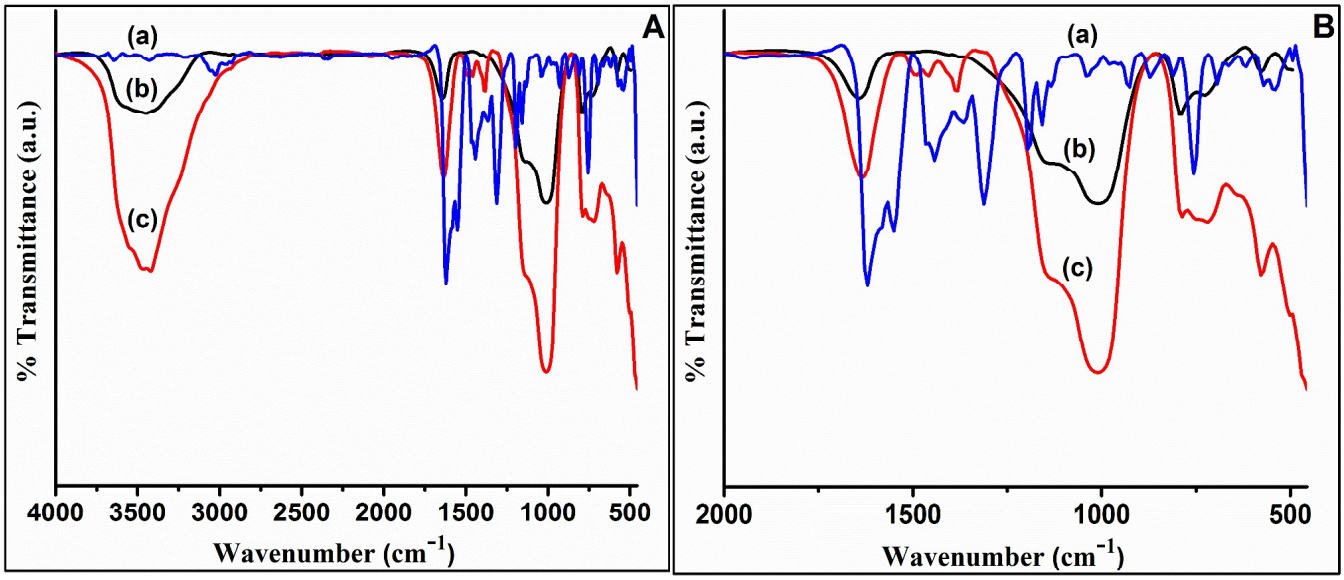

Figure 4.6: (A) FTIR spectra of (a) free-state cobalt salophen complex CoL1, (b) pure zeolite-Y and (c) encapsulated cobalt salophen complex CoL1-Y. (B) Enlarged view of FTIR spectra of (a) free-state CoL1 complex, (b) pure zeolite-Y and (c) encapsulated complex CoL1-Y.

Table 4.3: FTIR data of free-state and zeolite encapsulated complexes.

S. No	Samples	C=N stretching	C=C stretching	C-H deformation	C-O stretching
1	**CoL1**	1622	1548, 1464	1368	1307
2	**CoL1-Y**	1631	1492, 1458	1386	1276

4.2.7 X-ray Photoelectron Spectroscopy (XPS)

XPS results are shown in Figure 4.7-4.10 and Table 4.4. The XPS survey spectra of neat cobalt salophen complex suggest the presence of C (1s), N (1s), O (1s) and Co (2p) elements whereas in case of zeolite entrapped cobalt system, apart from these, some other characteristic peaks of Si (2p), Al (2p) and Na (1s) are also identified. Comparison of XPS signal intensity of Co (2p), indicates that encapsulated cobalt system has very low concentration of metal ions than that in the neat sample which is again in line with the results obtained from EDX, FTIR, TGA and UV-Vis studies.

In deconvoluted XPS spectrum of Co (2p) for CoL5, two XPS peaks appear at 780.52 eV and 795.62 eV corresponding to Co ($2p_{3/2}$) and Co ($2p_{1/2}$) respectively (Figure 4.8). Co (2p) peaks signifies that Co-species present in +2 oxidation state. However, a distinct variance is noticed in the high-resolution spectrum of Co (2p) of free-state and zeolite encapsulated cobalt complex. For encapsulated cobalt complex, the Co ($2p_{3/2}$) and Co ($2p_{1/2}$) signals are observed at 780.60 and 795.92 eV, respectively, as well as two shakeup satellite broad signals are also observed at 784.87 and 804.28 eV, respectively. This implies that the electronic environment around the metal center is altered and is in agreement with the literature reports.[39]

The high-resolution XPS spectra of C (1s) indicates three peaks located at 284.6 eV (C-C), 286.3 eV(C-O and 288.7 eV(C-N).[40] Deconvoluted N (1s) spectra represents two peaks at 399.52 and 402.22 eV are attributed to imine N (-C=N) atoms and some oxidized N atoms generated during XPS analysis upon irradiation with high energy X-rays. The high-resolution XPS spectrum of O (1s) have shown two XPS bands at 531.92 and 533.21 eV assigned to (M-O) and (C-O) oxygen atoms. XPS spectrum of zeolite encapsulated cobalt system indicates the presence of Si (2p), Al (2p) and Na (1s) observed at the binding energies of 103.22, 74.91 and 1072.83 eV respectively. XPS observations of zeolite entrapped cobalt system are quite consistent with those for their free-state analogues proving the successful formation of complex inside the supercage of zeolite Y.

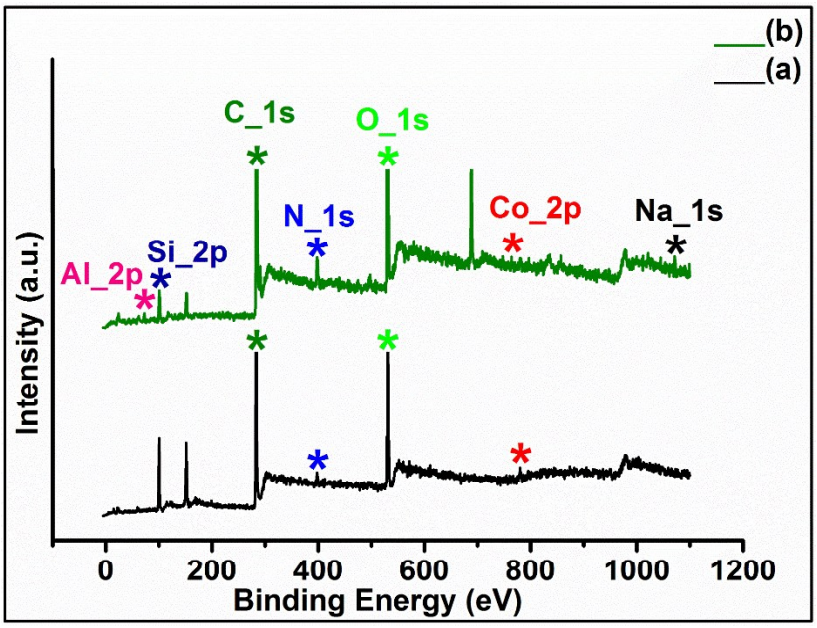

Figure 4.7: XPS survey spectra of (a) CoL5 and (b) CoL5-Y.

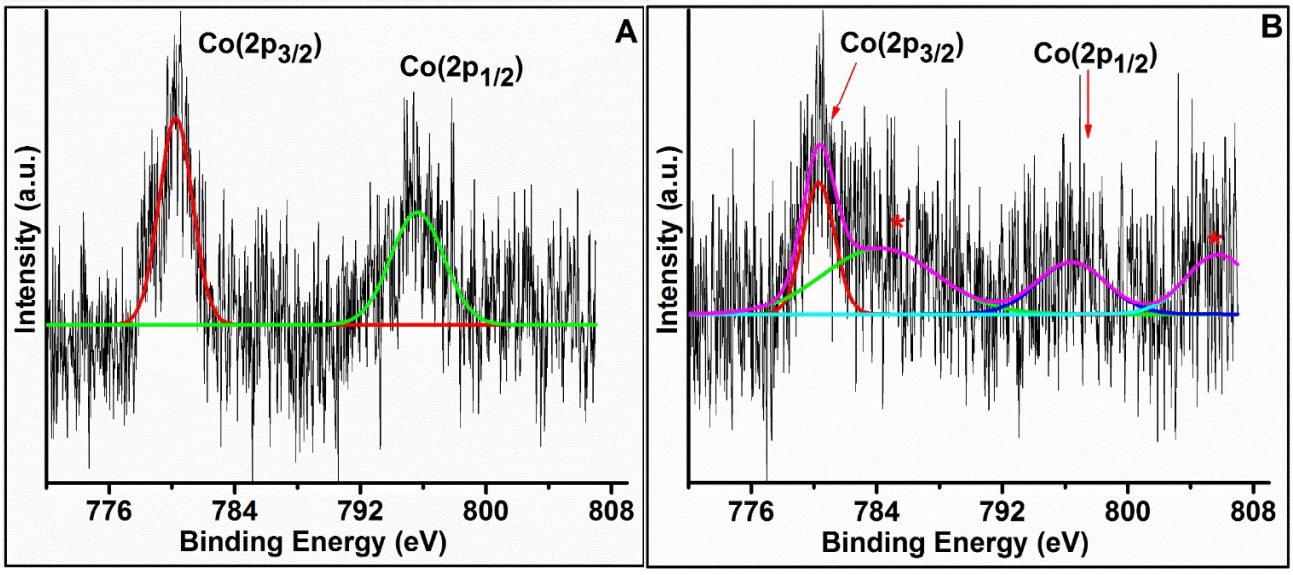

Figure 4.8: High-resolution XPS spectra for the Co (2p) signal (A) CoL5 and (B) CoL5- Y.

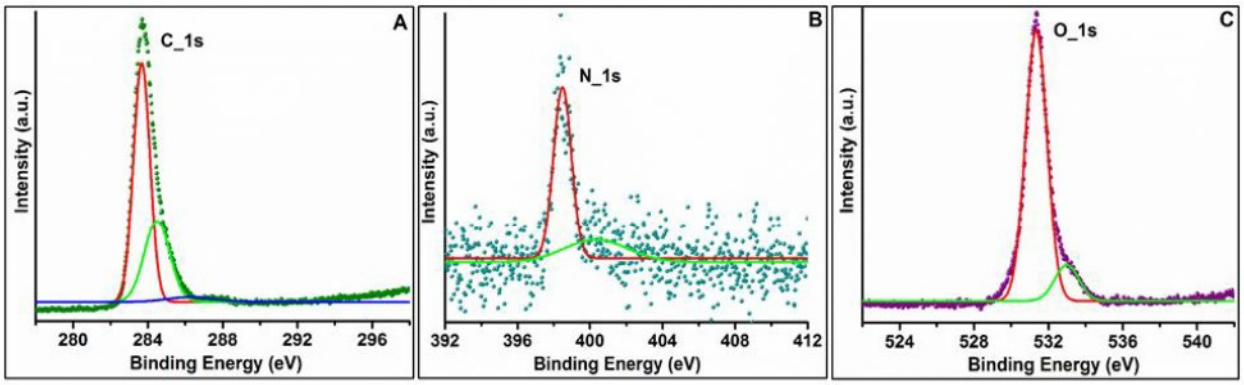

Figure 4.9: High-resolution peak fitted XPS spectra of (A) C (1s), (B) N (1s) and (C) O (1s) for CoL5.

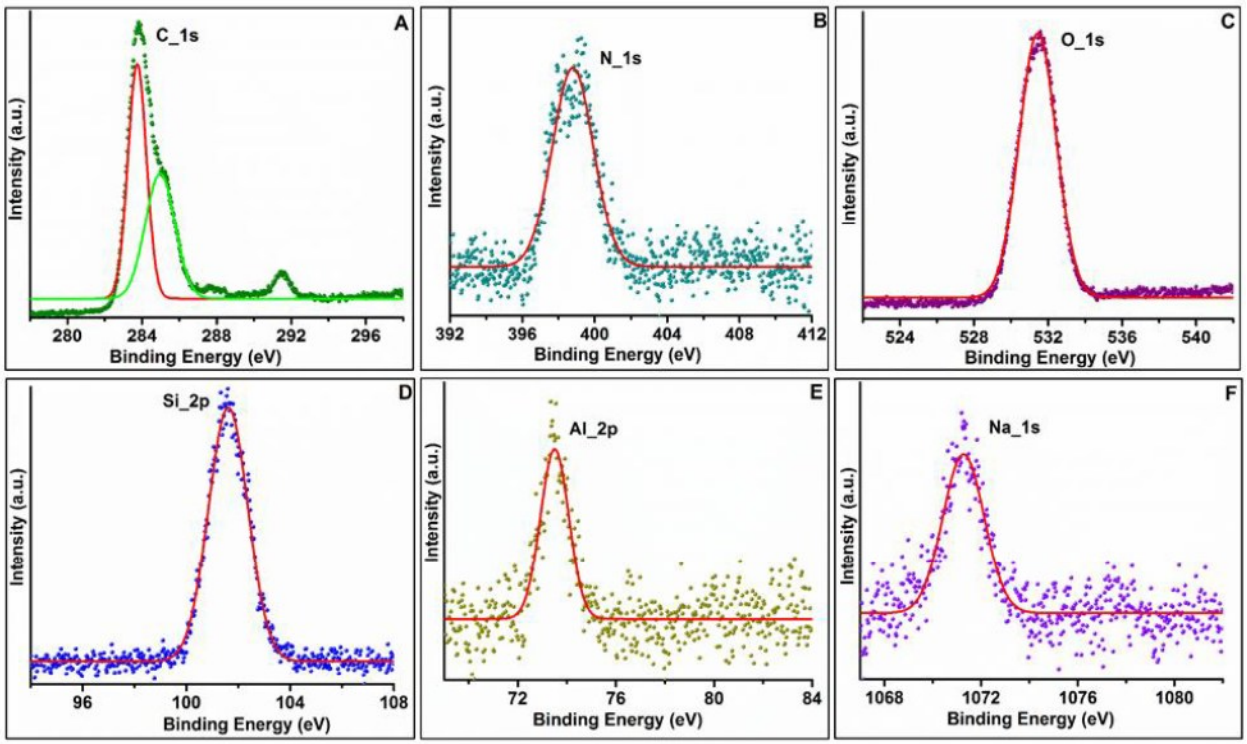

Figure 4.10: High-resolution XPS spectra of (A) C (1s), (B) N (1s), (C) O (1s), (D) Si (2p), (E) Al (2p) and (F) Na (1s) for CoL5-Y.

Table 4.4: Binding energy (eV) of neat and encapsulated complexes.

S. No	Samples	Si (2p)	Al (2p)	Na (1s)	C (1s)	N(1s)	O (1s)	Co ($2p_{3/2}$)	Co ($2p_{1/2}$)
1.	**CoL5**	-	-	-	283.65, 284.47, 287.27	398.47, 400.87	531.31, 533.01	780.52	795.62
3.	**CoL5-Y**	101.62	73.50	1071.29	283.72, 284.98, 287.55	398.79, 400.92	531.47, 533.12	780.60, 784.87	795.92, 804.28

4.2.8 UV-Vis/Diffuse Reflectance Spectroscopy (UV−Vis/ DRS)

Electronic spectroscopic studies (UV−Vis/Diffuse reflectance spectroscopy) appear to be very useful to comprehend the coordination environment and geometry around the metal center. Solution UV−Vis spectra of the ligands and neat Co(II) Schiff-base complexes are recorded in chloroform. The solution UV-Vis spectra are shown in Figure 4.11 and relevant data are given in Table 4.5. The free-state cobalt complex (CoL1) exhibits the four bands at 248, 302, 340, and 388 nm. The absorbance bands at 248 and 302 nm are assigned as π-π^* and 340 and 388 nm are assigned as n-π^* transitions. However, the UV-Vis bands at 440 and 583 nm are the transitions related to the meals and are clear evidence for the complex formation as these are absent in UV-Vis spectrum of the ligand (L1) .

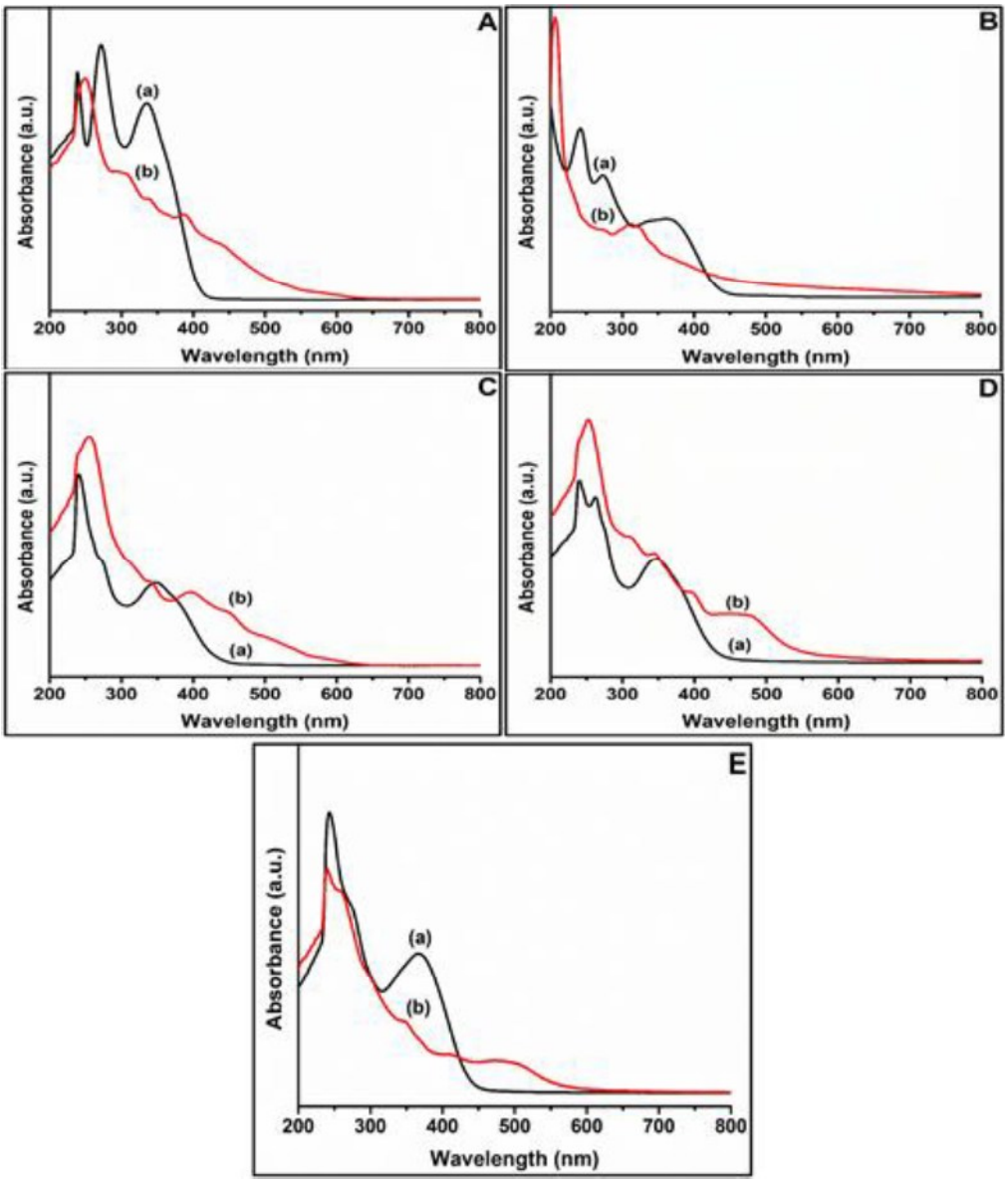

Figure 4.11: The solution UV-Vis spectra of Schiff-base ligands and Co(II) Schiff-base complexes (A) (a) L1 and (b) CoL1, (B) (a) L2 and (b) CoL2, (C) (a) L3 and (b) CoL3, (D) (a) L4 and (b) CoL4 and (E) (a) L5 and (b) CoL5.

Table 4.5: Solution UV-Visible data of ligand and neat complexes.

S. No	Samples	π—π^* transitions	n—π^* transitions	CT transitions / d-d transitions
1	**L1**	272, 283	335, 364	-
2	**CoL1**	248, 302	340, 388	440, 583
3	**L2**	241, 273	354, 370	-
4	**CoL2**	235, 271	315, 376	490, 596
5	**L3**	240, 271	349, 382	-
6	**CoL3**	255, 315	342, 396	502, 594
7	**L4**	239, 263	347, 385	
8	**CoL4**	238, 252	344, 396	478, 586
9	**L5**	244, 279	302, 375	
10	**CoL5**	239, 260	305, 350	500, 580

The comparative solid state UV-Vis spectra for the Co(II) Schiff-base complexes in both neat and encapsulated states are shown in Figure 4.12 along with the data tabulated in Table 4.6. UV-Vis bands in the range of (228-311) nm are characterized as π-π^* transitions, while the bands in the range of (322-405) nm are assigned as n-π^* transitions in solid state UV-Vis spectra of neat and encapsulated systems.[41] The complex formation in both the states is well-supported by the transitions observed in lower energy region of the UV-Vis spectrum as those are the metal related transitions. Absorbance bands occurred in the range of 402-589 nm and 492-590 nm are characterized as charge transfer and d-d transitions respectively.[42, 43] UV-Vis data of zeolite encapsulated cobalt systems are in well-agreement with that of their free state analogues, providing clear indication the successful complex formation inside the supercage of host framework.

Comparative electronic studies of the free state and encapsulated cobalt complexes show that the metal transitions (charge transfer and d-d transitions) are mainly altered under the encapsulation process, which indicate that coordination environment surrounding the metal center in the guest complex is largely affected upon encapsulation.

Interestingly, a similar prototype structural modification is observed for all the encapsulated Co(II) Schiff-base complexes. All encapsulated systems show a regular blue shift and intensification in the metal-related transitions. Such type of observations has been notified in zeolite encapsulated systems.[39] These modified electronic behavior of the metal complex is definitely the outcome of the modified coordination environment, especially around the metal center adopted by the guest complex due to the space constraints imposed by the supercage of host framework. End-to end dimension of All free state Co(II) Schiff-base complexes are comparable with the dimension of supercage. Therefore, guest cobalt complex experiences space constraint inside the supercage and eventually forced to adopt irregular geometries. Theoretical studies is very suggestive and supportive for such type of structural modifications. Amendment in various geometrical variables such as bond lengths, bond angles, and HOMO-LUMO gaps of guest metal complex are observed in the theoretical studies upon encapsulation.

Another fascinating observation is that as the guest metal complex with larger molecular dimension experiences more steric hindrance inside the host cavity. Therefore, higher extent of distortion becomes apparent so as to reduce the Vander waal interaction with the wall of zeolite Y. Consequently, blue shift is observed in d-d transition of the guest complex. Larger the molecular dimensions of the guest complexes, more is the blue shift observed.

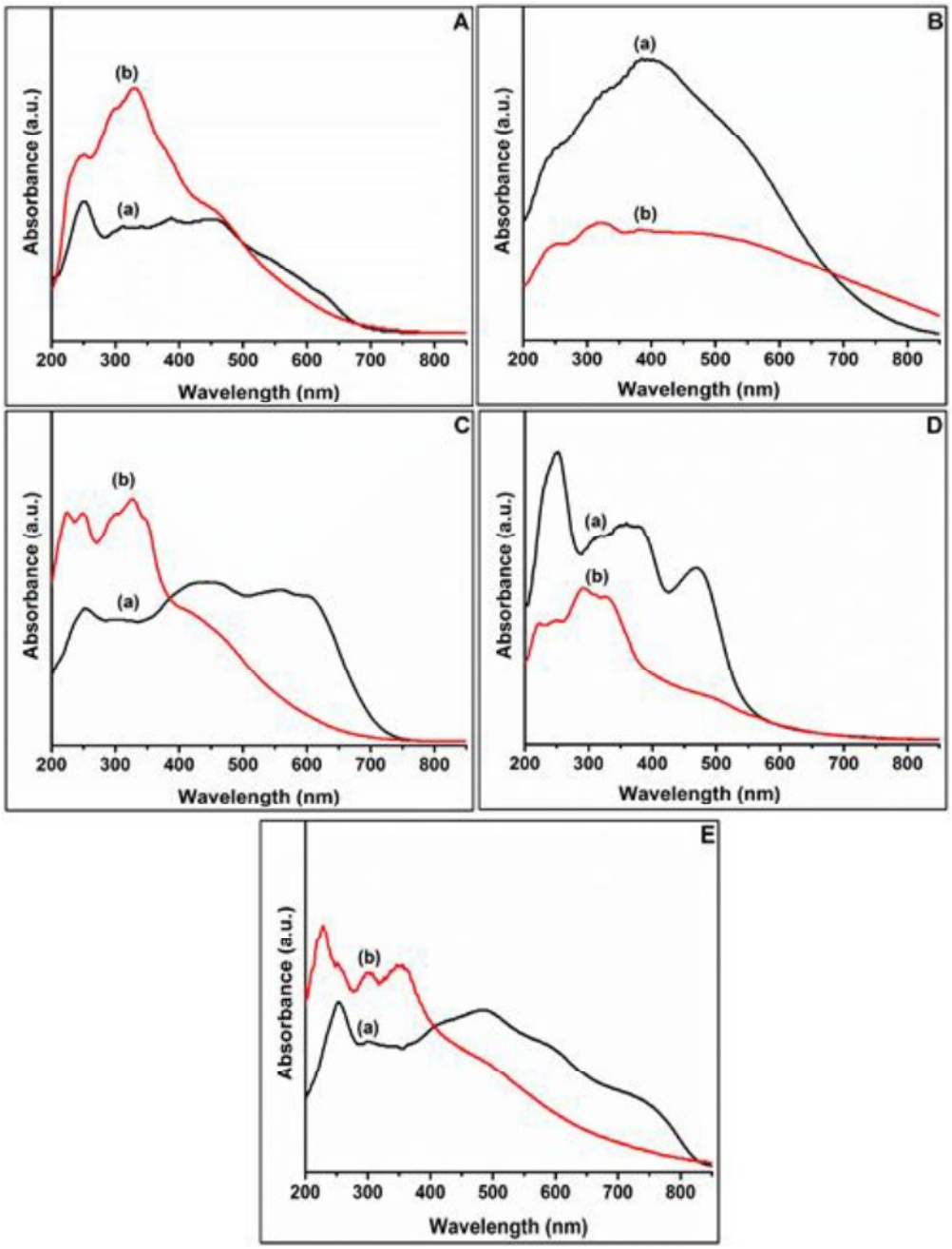

Figure 4.12: The Solid-state UV-Vis spectra of free-state and encapsulated Co(II) Schiff-base complexes (A) (a) CoL1 and (b) CoL1-Y, (B) (a) CoL2 and (b) CoL2-Y, (C) (a) CoL3 and (b) CoL3-Y, (D) (a) CoL4 and (b) CoL4-Y and (E) (a) CoL5 and (b) CoL5-Y.

Table 4.6: Solid-state UV-Visible data of neat and encapsulated complexes.

S. No	Samples	π—π^* transitions	n—π^* transitions	CT transitions / d-d transitions
1	**CoL1**	250, 311	387	466, 628
2	**CoL1-Y**	249, 299	328, 384	462, 620
3	**CoL2**	248	322, 389	537, 670
4	**CoL2-Y**	250	324, 384	530, 680
5	**CoL3**	251, 304	388	560, 608
6	**CoL3-Y**	223, 248	326	450, 600
7	**CoL4**	250, 311	360	469, 568
8	**CoL4-Y**	242, 289	328	495, 560
9	**CoL5**	252, 302	405	589, 726
10	**CoL5-Y**	228, 302	354	494, 672

4.2.9 Catalytic Study

Both, free state and encapsulated Co(II) Schiff-base complexes are employed as catalysts for the degradation of Rhodamine B dye in presence of UV light. The photocatalytic degradation has been performed in presence of H_2O_2 as oxidant. The degradation of dye has been monitored by using UV-Vis spectrophotometer at different time intervals within the range of 200-800 nm. The aliquot samples of the reaction mixture is collected at certain time intervals and spectral changes are analyzed at the wavelength of 554 nm (λ_{max} of rhodamine B dye). The percentage of the degradation has been calculated by using Lambert-Beers law-

($A = \varepsilon . c . l$) Here ε = molar extinction coefficient [M^{-1} cm^{-1}], c = concentration of sample, l = path length [cm].

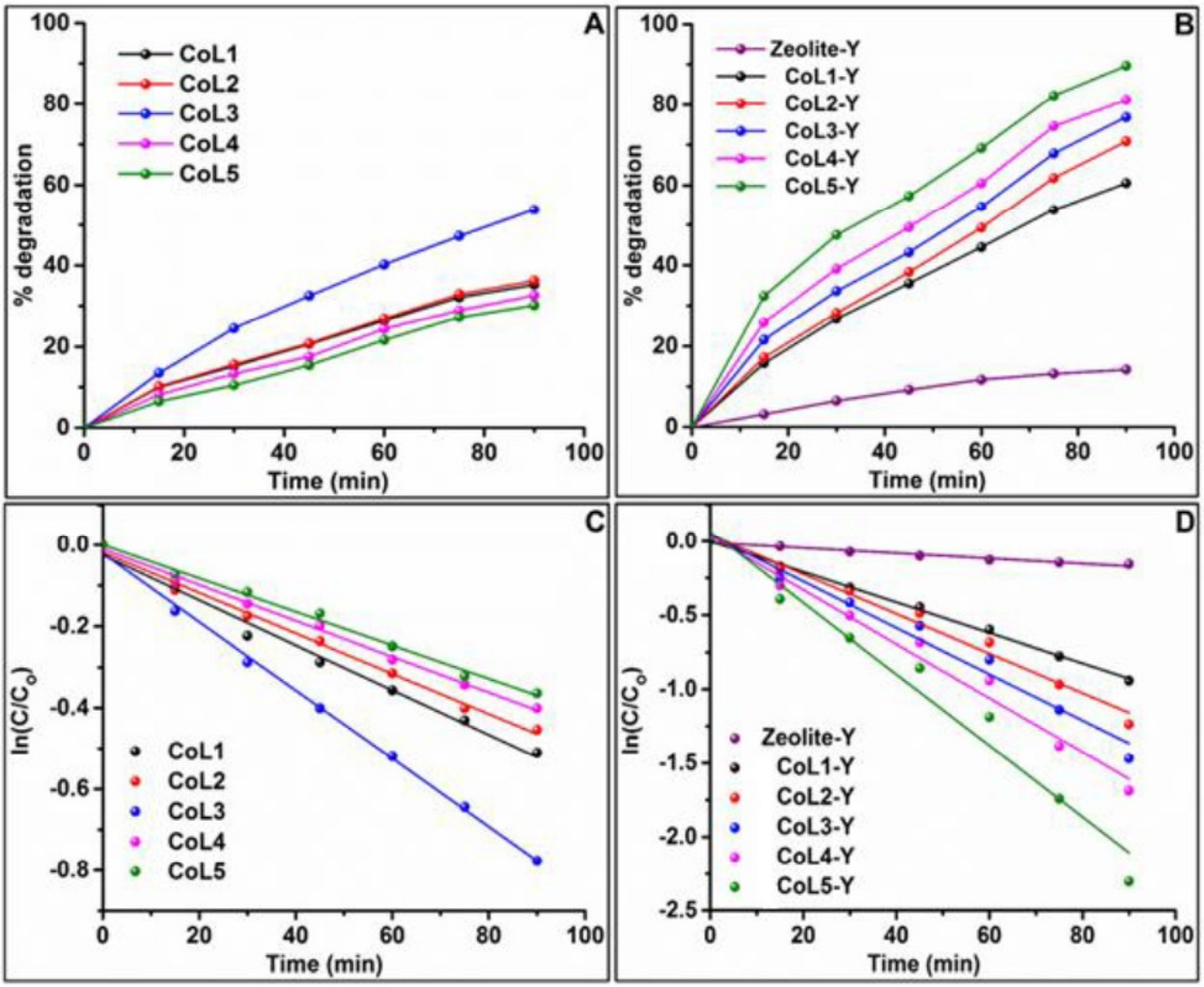

Figure 4.13: (A) and (B) Graphs of time vs. % degradation, and (C) and (D) kinetic plots for free-state and zeolite encapsulated cobalt complexes.

The results of RhB degradation are shown in Figure 4.13 and Table 4.7. From the dye degradation data, it is clearly evident that the zeolite encapsulated Co(II) Schiff-base complexes are more efficient as catalysts than their neat analogues.

Table 4.7: % degradation of rhodamine B after 1.5 h reaction time with H_2O_2 as oxidant.

S.No.	Catalyst	% Degradation	S.No.	Catalyst	% Degradation
1	**CoL1**	35.25	**6**	**CoL1-Y**	60.52
2	**CoL2**	36.20	**7**	**CoL2-Y**	72.85
3	**CoL3**	53.79	**8**	**CoL3-Y**	76.85
4	**CoL4**	32.58	**9**	**CoL4-Y**	81.10
5	**CoL5**	30.16	**10**	**CoL5-Y**	89.62

Reaction conditions: 0.02 mmol of 50 ml rhodamine B aqueous solution, H_2O_2 (0.88 mmol) and catalyst (0.0036 mmol for encapsulated and neat complexes).

4.2.10 Structural modification and photochemical performance

The photo catalytic degradation of the Rhodamine B when investigated in presence of neat and encapsulated cobalt systems under UV/Visible irradiation, blue shift in the λ_{max} of rhodamine B dye is observed. According to the literature,[44] this blue shift actually indicate the detachment of chromophoric group of dye molecules and formation of de-ethylated intermediates during the degradation of dye. The zeolite encapsulated cobalt systems are proven to be more active as catalyst as compared to free-state cobalt complexes and zeolite-Y. Encapsulated metal complexes inside the pores of zeolite probably facilitate the reaction by reducing the recombination of electron-hole pair. Production of hydroxyl radical ($^{\bullet}OH$) takes place rapidly due to the uniform distribution of cobalt metal inside the zeolite framework and hydroxyl radical is considering as effective oxidant (E^o = 2.8 V). Generation of $^{\bullet}OH$ radical is increased during metal reduction in presence of hydrogen peroxide. So, the catalytic efficiency depends upon the production of reactive ionic radicals such as $O_2^{\bullet-}$, ^{-}OOH, $^{\bullet}OH$ etc. Photogenerated $O_2^{\bullet-}$ and $^{\bullet}OH$ are very reactive radicals and these radicals quickly oxidize the organic species.

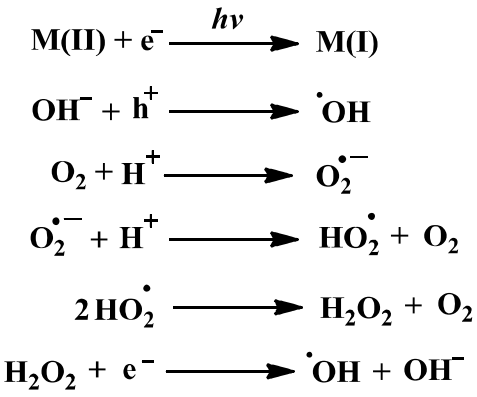

The order of photocatalytic activity for the free-state cobalt complexes is CoL5 < CoL4 < CoL1 ≤ CoL2 < CoL3. Here, CoL3 free state complex is most active among the all free state cobalt complexes as –Br group as a substituent makes the cobalt center more susceptible for the electrophilic attack Electron withdrawing -Br group in CoL3 makes the system non planar as well and hence more electropositive metal centre. Strong electron donating $–OCH_3$ group in CoL5 makes the system planar and less susceptible cobalt centre for the electrophilic attack and subsequently least reactive among all neat cobalt complexes. On the other hand, CoL2 complex shows slightly greater reactivity than expected, the reason could be the better solubility of the complex in the reaction medium.

Encapsulation of these cobalt Schiff-base complexes inside the supercage of zeolite -Y further improves the extent of distortion and makes the metal more electropositive and subsequently more reactive. Largest complex upon encapsulation, undergoes more distortion and has manifested highest reactivity among all free-state and encapsulated systems for dye degradation. Quite interestingly, this complex is found least reactive for the same reaction in its free state. For the encapsulated Co(II) Schiff-base complexes, the reactivity order is mainly driven by the molecular dimension and degree of distortion of the guest complex which has been established by the electronic spectroscopy. The reactivity order for the encapsulated systems becomes CoL5-Y > CoL4-Y > CoL3-Y > CoL2-Y > CoL1-Y, whereas the free-state complexes show the order as: CoL5 < CoL4 < CoL1 ≤ CoL2 < CoL3. More electropositive metal centre is more accessible for the electron. However, the reduction of electron density can be attained by the addition of electron withdrawing group or by the structural modification upon encapsulation in zeolite-Y.

4.3 CONCLUSION

A series of free-state Co(II) salophen complexes and their encapsulated analogues have been synthesized by using flexible ligand method. Characterization of the synthesized materials has been done by the help of various spectroscopic, sorption and microscopic techniques and thermal analysis. Catalytic activity of the free-state and zeolite encapsulated cobalt systems have been studied for the degradation of rhodamine B dye. In the photocatalytic degradation of rhodamine B dye, degradation percentage depends on the photo generated oxidants, which are interact with metal species. As a result, a cascade of oxidation reactions are started which can degrade the organic dye.

Zeolite framework delivers a route to design the heterogeneous catalyst with modified reactivity by the encapsulation of metal complex. Walls of zeolite framework enforce space constraints on the guest metal complex. Consequently, the guest metal complex adopt a modified geometry. Such type of structural modifications recognized by the help of shift in metal transition in electronic spectra. These structural modifications play a key role for the modified reactivity of the systems. The guest complex along with larger molecular dimension experiences more strain inside the supercage of zeolite-Y. As a result, the structure of guest complex becomes more distorted and consequences create the more reactive metal center in the encapsulated system.

4.4 REFERENCES

1. S. Horikoshi, F. Hojo, H. Hidaka and N. Serpone, *Environ. Sci. Technol.*, 2004, **38**, 2198-2208.
2. P. Gamez, P. G. Aubel, W. L. Driessen and J. Reedijk, *Chem. Soc. Rev.*, 2001, **30**, 376-385.
3. M. L. Marin, L. Santos-Juanes, A. Arques, A. M. Amat and M. A. Miranda, *Chem. Rev.*, 2011, **112**, 1710-1750.
4. J.-M. Brégeault, *Dalton Trans.*, 2003, 3289-3302.
5. D. Habibi, A. R. Faraji, M. Arshadi and J. L. G. Fierro, *J. Mol. Catal. A: Chem.*, 2013, **372**, 90-99.
6. J. Jiang, R. Babarao and Z. Hu, *Chem. Soc. Rev.*, 2011, **40**, 3599-3612.
7. B. Agboola, K. I. Ozoemena and T. Nyokong, *J. Mol. Catal. A: Chem.*, 2005, **227**, 209-216.
8. G. R. Reddy, S. Balasubramanian and K. Chennakesavulu, *J. Mater. Chem. A*, 2014, **2**, 15598-15610.
9. A. C. Pradhan, B. Nanda, K. Parida and M. Das, *Dalton Trans.*, 2013, **42**, 558-566.
10. X.-J. Hong, X. Liu, J.-B. Zhang, C.-L. Lin, X. Wu, Y.-J. Ou, J. Yang, H.-G. Jin and Y.-P. Cai, *CrystEngComm*, 2014, **16**, 7926-7932.
11. E. N. Jacobsen, *Catal. Asymmetric Synth.*, 1993, 159-202.
12. E. N. Jacobsen, *Acc. Chem. Res.*, 2000, **33**, 421-431.
13. P. G. Lacroix, *Eur. J. Inorg. Chem.*, 2001, **2001**, 339-348.

14. H. Andres, R. Basler, A. J. Blake, C. Cadiou, G. Chaboussant, C. M. Grant, H.-U. Güdel, M. Murrie, S. Parsons, C. Paulsen, F. Semadini, V. Villar, W. Wernsdorfer and R. E. P. Winpenny, *Chem. - Eur. J.*, 2002, **8**, 4867-4876.
15. A. Staykov, M. Watanabe, T. Ishihara and K. Yoshizawa, *J. Phys. Chem. C*, 2014, **118**, 27539-27548.
16. V. Nishal, D. Singh, R. K. Saini, V. Tanwar, S. Kadyan, R. Srivastava and P. S. Kadyan, *Cogent Chem.*, 2015, **1**, 1079291.
17. L.-L. Fan, F.-S. Guo, L. Yun, Z.-J. Lin, R. Herchel, J.-D. Leng, Y.-C. Ou and M.-l. Tong, *Dalton Trans.*, 2010, **39**, 1771-1780.
18. A. Saroja and B. R. Bhat, *Ind. Eng. Chem. Res.*, 2018, **58**, 590-601.
19. M. Chen, K. Peng, H. Wang, Z. Yang, Q. Zeng and A. Xu, *Chem. Eng. J.*, 2012, **197**, 110-115.
20. M. Ghiyasiyan-Arani, M. Masjedi-Arani and M. salavati-Niasari, *J. Mol. Catal. A: Chem.*, 2016, **425**, 31-42.
21. W. Chen, W. Lu, Y. Yao and M. Xu, *Environ. Sci. Technol.*, 2007, **41**, 6240-6245.
22. J. Wöltinger, J. E. Bäckvall and Á. Zsigmond, *Chem. - Eur. J.*, 1999, **5**, 1460-1467.
23. P. Manna, J. Debgupta, S. Bose and S. K. Das, *Angew. Chem., Int. Ed.*, 2016, **55**, 2425-2430.
24. M. Salavati-Niasari and A. Sobhani, *J. Mol. Catal. A: Chem.*, 2008, **285**, 58-67.
25. D. Srinivas and S. Sivasanker, *Catal. Surv. Asia*, 2003, **7**, 121-132.
26. D. E. De Vos, B. F. Sels and P. A. Jacobs, *Cattech*, 2002, **6**, 14-29.
27. R. F. Parton, I. F. Vankelecom, M. J. Casselman, C. P. Bezoukhanova, J. B. Uytterhoeven and P. A. Jacobs, *Nature*, 1994, **370**, 541.
28. T. Sawano, N. C. Thacker, Z. Lin, A. R. McIsaac and W. Lin, *J. Am. Chem. Soc.*, 2015, **137**, 12241-12248.
29. M. Salavati-Niasari, M. Shakouri-Arani and F. Davar, *Microporous Mesoporous Mater.*, 2008, **116**, 77-85.
30. C. Modi and P. M. Trivedi, *Adv. Energy Mater.*, 2014, 555-583.
31. W. H. Quayle and J. H. Lunsford, *Inorg. Chem.*, 1982, **21**, 97-103.
32. W. H. Quayle, G. Peeters, G. L. De Roy, E. F. Vansant and J. H. Lunsford, *Inorg. Chem.*, 1982, **21**, 2226-2231.
33. Y. Umemura, Y. Minai and T. Tominaga, *J. Phys. Chem. B*, 1999, **103**, 647-652.
34. K. K. Bania and R. C. Deka, *J. Phys. Chem. C*, 2012, **116**, 14295-14310.
35. H. S. Abbo and S. J. Titinchi, *Top. Catal.*, 2010, **53**, 1401-1410.
36. A. N. Parikh, A. Navrotsky, Q. Li, C. K. Yee, M. L. Amweg and A. Corma, *Microporous Mesoporous Mater.*, 2004, **76**, 17-22.
37. S. C. Mohan, R. Vijay Solomon, P. Venuvanalingam and K. Jothivenkatachalam, *New J. Chem.*, 2017, **41**, 9505-9512.
38. M. Maurya, S. Titinchi, S. Chand and I. Mishra, *J. Mol. Catal. A: Chem.*, 2002, **180**, 201-209.
39. A. Choudhary, B. Das and S. Ray, *Dalton Trans.*, 2015, **44**, 3753-3763.
40. T. Zhang, C. He, F. Sun, Y. Ding, M. Wang, L. Peng, J. Wang and Y. Lin, *Sci. Rep.*, 2017, **7**, 43638.
41. A. Böttcher, T. Takeuchi, K. I. Hardcastle, T. J. Meade, H. B. Gray, D. Cwikel, M. Kapon and Z. Dori, *Inorg. Chem.*, 1997, **36**, 2498-2504.
42. P. R. Blum, R. M. C. Wei and S. C. Cummings, *Inorg. Chem.*, 1974, **13**, 450-456.
43. M. Salavati-Niasari, *J. Mol. Catal. A: Chem.*, 2008, **283**, 120-128.
44. H. Fu, C. Pan, W. Yao and Y. Zhu, *J. Phys. Chem. B*, 2005, **109**, 22432-22439.